

## RECYCLING NEUTRON STARS TO ULTRASHORT PERIODS: A STATISTICAL ANALYSIS OF THEIR EVOLUTION IN THE $\mu$ - $P$ PLANE

ANDREA POSSENTI,<sup>1</sup> MONICA COLPI,<sup>2</sup> ULRICH GEPPERT,<sup>3</sup> LUCIANO BURDERI,<sup>4</sup> AND NICHÌ D'AMICO<sup>5</sup>

Received 1999 April 19; accepted 1999 July 26

### ABSTRACT

In this paper we investigate the statistical evolution of magnetic neutron stars, recycled in binary systems, simulating synthetic populations. To bracket uncertainties, we consider a soft (FP) and a stiff (PS) equation of state (EoS) for nuclear matter and explore the hypothesis that the magnetic field is confined in the stellar crust. We follow the magnetorotational evolution within a simple recycling scenario. The decay of the magnetic field is modeled imposing at the crust-core boundary either complete field expulsion by the superconducting core or advection and freezing in a very highly conducting transition shell. Irrespective of the details of the physical models, we find the presence of a tail in the period distribution of the synthetic populations at periods shorter than 1.558 ms, the minimum detected so far. For the soft EoS, and independent of the details of the magnetic field evolution, the recycling gives rise to a spin distribution that is increasing monotonically toward short periods, and a clear “barrier” forms at the minimum period for the onset of mass shedding ( $\approx 0.7$  ms). For the stiff EoS, the distribution is flatter, displaying a broad maximum about 2–4 ms. On the other hand, if in low-mass binaries the neutron stars experience a progressive decrease of the mass accretion rate (due to transient behavior and/or the quenching of accretion), the magnetospheric propeller produces (together with the magnetic dipole losses) an overall depletion of neutron stars in the millisecond region of the  $\mu$ - $P$  plane. The estimated fraction of neutron stars spinning close to their shedding limit over the millisecond pulsar population is found to be significant. Crustal magnetic field decay models also predict the existence of massive rapidly spinning neutron stars with very low magnetic moment  $\mu < 10^{25.8}$  G cm<sup>3</sup>.

*Subject headings:* equation of state — stars: magnetic fields — stars: neutron

### 1. INTRODUCTION

PSR 1937 + 21, at present, is the neutron star (NS) having the shortest rotational period  $P_{\min} = 1.558$  ms ever detected: it is a millisecond radio pulsar (MSP), the fastest among the  $\sim 30$  discovered in the Galactic field with weak magnetic field and age greater than  $10^9$  yr. Despite its apparent smallness,  $P_{\min}$  is not a critical period for NS rotation: NSs can indeed spin faster, as indicated by Cook, Shapiro, & Teukolsky (1994). These authors showed that during recycling a bare nonmagnetic NS can attain periods as short as  $P_{\min}$  with modest values of the rotational-to-potential energy ratio and modest values of the mass accreted ( $< 0.1 M_{\odot}$ ), for all known equations of state (EoSs) of the nuclear matter. The period  $P_{\min}$  is longer than the limiting period,  $P_{\text{sh}}$ , below which the star becomes unstable to mass shedding at its equator, irrespective of the EoS. It is clear that only the discovery of an ultrashort-period MSP (i.e., a weak field pulsar with  $P$  close to  $P_{\text{sh}}$ ) would allow us to set limits on the proposed EoSs; as an example, a very soft EoS permits pulsations at  $\sim 0.7$  ms.

Burderi et al. (1999) noticed that the recycling of magnetic NSs to  $P < 10$  ms depends sensitively on the mass transferred to the compact object and crucially on the evolution

of the surface magnetic field. In particular, a slowly decaying magnetic field favors only the reacceleration of a NS to  $P \gtrsim 5$ –10 ms, while halving the request of mass accreted with respect to the case of a nonmagnetic star. Conversely, if a rapid and substantial decay of the surface magnetic field takes place, a NS can attain  $P < P_{\min}$ . In this case, the minimum mass load necessary to approach  $P_{\text{sh}}$  is  $\sim 0.3 M_{\odot}$ : it was calculated using the softest EoS (having  $P_{\text{sh}} = 0.7$  ms) and introducing the most favorable ad hoc evolution for the decay of the magnetic field. In this paper we wish to study in detail those processes that interfere positively to spin up a NS up to  $P_{\text{sh}}$  in a low-mass binary (LMB). Among them, the most important are the evolution of the magnetic moment  $\mu$  and the evolution of the mass transfer.

At present, there is no satisfactory theory for the origin of the magnetic field, and consequently several avenues of field decay are possible: the field can either be a fossil remnant from the progenitor star or be generated soon after the formation of the NS. Thus, an unanswered question is where the bulk of the magnetic energy is stored (Bhattacharya & Srinivasan 1995). If it resides mainly in the core (as in the case of a fossil field), the evolution of  $\mu$  may be driven by variations in the rotational state of the NS, which affects the motion of the superfluid vortices and, in turn, of the fluxoids, carriers of the magnetic energy (Srinivasan et al. 1990; Ding, Chen, & Cau 1993; Miri & Bhattacharya 1994; Ruderman, Zhu, & Chen 1998). If the magnetic energy is generated and confined in the thin crust of the NS (Blandford, Applegate, & Hernquist 1983; Urpin, Levshakov, & Yakovlev 1986), the surface magnetic field decay is guided by the ohmic diffusion and the dissipation of electric currents (Sang & Channugam 1987: see § 3 for an updated set of references). The EoS valid for the core determines the thickness of the crust as well as the cooling

<sup>1</sup> Dipartimento di Astronomia dell'Università, via Ranzani 1, 40127 Bologna, Italy.

<sup>2</sup> Dipartimento di Fisica dell'Università, via Celoria 16, 20133 Milano, Italy.

<sup>3</sup> Astrophysikalisches Institut Potsdam, An der Sternwarte 16, 14482 Potsdam, Germany.

<sup>4</sup> Osservatorio Astronomico di Monteporzio, via Frascati 33, 00044 Roma, Italy.

<sup>5</sup> Osservatorio Astronomico di Bologna, via Ranzani 1, 40127 Bologna, Italy.

history of the NS, both of which affect strongly the magnetic field decay. In the case of a crust field, however, magnetic evolution is not univocal, depending sensitively on the properties of the nuclear matter at the crust-core boundary, where superfluid (SF) and superconductive (SC) phase transitions may occur. As crustal matter is progressively assimilated into the core owing to accretion, the magnetic field at the crust-core boundary can either be expelled (Urpin, Geppert, & Kononov 1998a) or advected into the SC core where it no longer decays (Konar & Bhattacharya 1998). Thus, at the endpoint of evolution, the NS can either become nonmagnetic (on the long term) or preserve a relic field intense enough to shine again as an MSP. These avenues are possible and the extent of the decay is intimately connected with the transfer rate and amount of matter accreted as heat released in the crust raises the electron and ion resistivity, accelerating the dissipation of current. Thus, field and mass transfer evolution couple intimately during the lifetime of the NS in a LMB.

Within the recycling scenario (Alpar et al. 1982; Bhattacharya 1995) all schemes suggested for the origin and the evolution of  $\mu$  allow accreting NSs to reduce their magnetic moment to the values that are characteristic of MSPs (Urpin et al. 1998a), but core models require rather extreme conditions on the impurity content of crustal matter (Konar & Bhattacharya 1999). Only through a statistical approach is it possible to establish how efficient the recycling process is in spinning NSs to ultrashort periods. This was recognized first by Possenti et al. (1998, hereafter Paper I) who carried on a statistical analysis of NSs in the millisecond and submillisecond interval, using a population synthesis model. Their aim was to determine whether there might exist feasible conditions for spinning a significant number of NSs to  $P < P_{\min}$ , during recycling in LMBs. They found the first evidence of a tail in the distribution of MSPs at periods shorter than those detected so far. This possibility was met within empirical models that involve the screening by the accreting matter treated as a pure diamagnet (Bisnovatyi-Kogan & Komberg 1975) and models that call for a crustal nature of the magnetic field.

In this paper we modify the population synthesis calculation of Paper I incorporating a detailed physical model for the evolution of a crustal magnetic field (using two boundary conditions to mimic expulsion or assimilation of the field by the SC core), adding further effects that might alter the statistical outcome. We also improve accuracy including the relativistic corrections (Burderi et al. 1999) necessary to describe the spin-up process when the NS accretes matter from a disk, whose inner rim approaches the radius of the last quasi-stable orbit.

The evolution in the  $\mu$ - $P$  plane is followed within a scenario of recycling, constructed using our knowledge of accretion in low-mass X-ray binaries (LMXBs). The study is not aimed at correlating, on an evolutionary level, the observed population of LMXBs with the observed population of MSPs. MSPs may not be indeed the direct descendant of LMXBs: establishing this potential link or the link with LMBs forming through alternative evolutionary channels (Kalogera & Webbink 1996, 1998) would require the complete statistical knowledge of the orbital parameters, of the mass ratios, of the hydrodynamical processes guiding mass transfer, and ultimately of the internal evolution and structure of the donor star (see, e.g., Ergma, Sarna, & Antipova 1998; Muslimov & Sarna 1993). These are aspects of a

complex statistical calculation that is beyond our purposes. We wish here to determine whether a minimal but possibly physically consistent model for the recycling can provide indications of the period distribution of NSs in the millisecond and submillisecond domain, as a guideline for future searches. Our aim is also to address a number of questions that we are outlining below.

In our population synthesis model we account for the evolution during the early phases when the NS in the LMB behaves as if isolated and later when fed by wind accretion. The mass transfer during the Roche lobe overflow (RLO) phase is modeled just considering a range of accretion rates that is close to the one observed in LMXBs (Frank, King, & Raine 1992; Webbink, Rappaport, & Savonije 1983). In a number of models, the accretion rate is treated as a constant over the RLO phase: this is an approximation as its actual behavior follows a complex evolutionary pattern depending on the orbital parameters and on the degree of mass and orbital angular momentum losses (Ergma et al. 1998; Ergma & Sarna 1996).

The increasing evidence that NSs in LMXBs may suffer phases of transient accretion owing to thermal viscous instabilities in an irradiation-dominated disk (e.g., van Paradijs 1996; King, Kolb, & Szuszkiewicz 1997b; King et al. 1997a) is suggestive that mass transfer onto a NS may not stop suddenly, at the end of the RLO: the star probably undergoes a progressive reduction of the mean accretion rate, modulated by alternate phases of higher and lower accretion. The effects of this transient behavior on the evolution of the magnetic field is not known yet (D. Page, M. Colpi, U. Geppert, & A. Possenti 2000, in preparation), but, if the magnetic field is not too weak, any drop in the accretion rate implies the growth of the typical dimension of the magnetosphere (Bhattacharya & van den Heuvel 1991; see § 2 for details). Dragged by the rapidly spinning NS, the magnetosphere can transform in a centrifugal barrier, accelerating the matter at the inner rim of the accretion disk on super-Keplerian orbits (propeller effect: Illarionov & Sunyaev 1975); the extraction of angular momentum from the compact object that follows spins down the NS. *Does unsteady accretion at the end of the RLO phase vanish the effect of the previous phases of spin-up? Is the potential population of very rapidly spinning NSs reflected back to  $P > P_{\min}$ ? Many physical ingredients necessary to describe fully the propeller-induced spin-down are poorly known or are difficult to assess (e.g., the exact law for the decrease of the mass transfer rate or the efficiency in the extraction of the angular momentum from the NS to the propelled matter). So, we studied the problem on a statistical basis, parameterizing the most uncertain quantities.*

The fastest rotating NSs detected so far have been discovered at radio frequencies, and statistical analyses based on current samples of MSPs (Cordes & Chernoff 1997) have revealed that the pulsar distribution is increasing toward short periods with best-fit minimum period slightly below  $P_{\min}$ . Radio searches for very rapidly spinning objects are now in progress. In particular the large-scale survey at the Northern Cross Radiotelescope near Medicina (D'Amico et al. 1998) has a sensitivity profile relatively flat in the submillisecond period range. If successful, these searches can potentially provide information on the EoS for nuclear matter (Burderi & D'Amico 1997; Phinney & Kulkarni 1994; Stergioulas & Friedman 1995). If NSs can be recycled up to  $P_{\text{sh}}$ , the observed population can retain features of the

EoS. Yet, many factors influence the recycling process (magnetic moment evolution, total amount of mass available for the accretion, evolution of the mass transfer rate, propeller induced spin-down, and so on) likely spreading the observed distribution to slower spin rates and perhaps, in extreme cases, almost completely masking the effects of the EoS. Thus, *can we determine, on a statistical basis, whether recycled rapidly rotating pulsars preserve signatures, in their  $\mu$ - $P$  diagram, for a distinction between the EoSs?*

Both types of evolution for a magnetic field of crustal origin allow, to a different degree, for the decay of  $\mu$  at values lower than those typical of the observed MSPs sample and probably below the threshold for radio emission (Konar & Bhattacharya 1998; Geppert & Kononkov 1998; Sturrock 1971; Ruderman & Sutherland 1975). In view of these searches an additional question is worth exploring: *Can we find a distinct feature in the distribution of NSs reflecting the boundary conditions at the crust-core interface? How significant is the production of weakly magnetized NSs during recycling?* As with the previous case, the statistical approach will help in clarifying whether the behavior of highly condensed matter can be inferred from a close analysis of the NS period distribution.

In § 2 we outline the magnetorotational evolution of a NS as predicted by the recycling scenario, introducing the parameters adopted for the calculation. In § 3 we focus on the evolution of the magnetic field residing in the crust of an accreting NS and describe the effects of different physical assumptions. In § 4 we present the results of the population synthesis calculations, addressing one by one the questions raised in § 1. Section 5 contains the conclusions.

## 2. SPIN EVOLUTION SCENARIO

### 2.1. Physical Model

According to the recycling scenario (e.g., Lipunov 1992), the NSs in low-mass binaries (LMBs) may experience the phase of ejector, accretor, or propeller. In the ejector phase, the NS spins down only via radiation torque, and we assume dipole emission according to the simple law

$$\dot{P} = 3.15 \times 10^{-16} \frac{\mu_{26}^2}{P} \text{ s yr}^{-1}, \quad (1)$$

where  $P$  is the neutron star rotation period in seconds and  $\mu_{26}$  is the magnetic moment in units of  $10^{26} \text{ G cm}^3$ .

In the propeller and accretor phases, matter penetrates down to the NS magnetosphere whose radius (Bhattacharya & van den Heuvel 1991) is

$$r_{\text{mag}} = 9.8 \times 10^5 \phi \mu_{26}^{4/7} \dot{m}^{-2/7} M^{-1/7} R_6^{-2/7} \text{ cm}, \quad (2)$$

where  $\phi$  is estimated following Burderi et al. (1998); in equation (2),  $M$  is the NS mass in solar masses,  $R_6$  is the static NS equatorial radius in units of  $10^6 \text{ cm}$ , and  $\dot{m}$  the accretion rate in units of Eddington, i.e.,  $1.5 \times 10^{-8} R_6 M_\odot \text{ yr}^{-1}$ . In the propeller state, the uniform angular velocity of the NS is higher than the Keplerian velocity at  $r_{\text{mag}}$ , and the magnetosphere acts as a centrifugal barrier (Illarionov & Sunyaev 1975). The infalling plasma is forced into super-Keplerian rotation and is propelled away: the NS loses angular momentum and spins down. The accretion phase sets in every time the magnetosphere does not act as a barrier to matter approaching  $r_{\text{mag}}$ . In the statistical analysis of the RLO phase, we assume that the NS is fed through a disk whose inner radius  $r_{\text{in}}$  depends on the magnetic and rota-

tional parameters of the NS. For high enough  $\mu$ , the magnetic coupling between the disk and the star determines the extent of the angular momentum transfer: the corresponding value of  $r_{\text{in}}$  is  $r_{\text{mag}}$ . In general  $r_{\text{mag}}$  must be compared with both  $R_\Omega$  and  $r_{\text{ms}}$ , where  $R_\Omega$  is the physical equatorial radius of the NS (accounting for the inflation due to very fast rotation), and  $r_{\text{ms}}$  is the radius of the last stable orbit. If the magnetic field is very low ( $\mu \lesssim 10^{26.5} \text{ G cm}^3$ ),  $r_{\text{mag}}$  is smaller than  $R_\Omega$  (or  $r_{\text{ms}}$ ), and the accretion disk is truncated directly at the NS surface ( $r_{\text{in}} = R_\Omega$ ) or at the last stable orbit ( $r_{\text{in}} = r_{\text{ms}}$ ).

The angular momentum balance relation used to follow the period evolution of the NS is

$$\frac{d(I_\Omega \Omega)}{dt} = g \dot{m} l_{\text{in}}, \quad (3)$$

where  $I_\Omega$  is the moment of inertia of the rotating star,  $\Omega$  is its angular velocity, and  $l_{\text{in}}$  is the specific angular momentum of the accreting matter at the relevant inner radius  $r_{\text{in}}$  of the disk. The torque function  $g = g(\Omega)$  accounts for the details of the angular momentum transfer between the NS magnetosphere and the accretion disk. When  $r_{\text{in}} = r_{\text{mag}}$  and  $g = 0.0$ , the NS is on the so-called spin-up line, where it can accrete mass without modifying its angular momentum  $I_\Omega \Omega$ . If the magnetospheric radius is inside the marginally stable radius  $r_{\text{ms}}$  or inside the star's radius, we set  $r_{\text{in}} = r_{\text{ms}}$  (or  $= R_\Omega$ ), and  $g$  is equal to 1. When the NS is in a propeller state, the function  $g$  becomes negative (see § 2.2 for the values adopted). If the position of the NS in the  $\mu$ - $P$  plane at the end of mass transfer is above the "death line" (Sturrock 1971; Ruderman & Sutherland 1975), the NS shines as a *pulsar* and suffers secular spin-down by magnetic dipole torques (eq. [1]). In this terminal phase, the pulsar migrates to the right of the  $\mu$ - $P$  diagram, drifting toward longer periods.

### 2.2. Values Adopted for the Synthesized Populations

The NSs evolved in our population synthesis model have an initial gravitational mass of  $1.4 M_\odot$ . Cook et al. (1994) showed that all viable equations of state (EoSs) for nuclear matter allow for recycling a  $1.4 M_\odot$  unmagnetized NS to ultrarapid spinning rates. Values of  $P \lesssim 1.5 \text{ ms}$  are attained (before the mass-shedding instability disrupts the star) even in those models having a static maximum mass close to  $1.4 M_\odot$ . However, the minimum attainable period depends on the specific equation of state. We here investigated two EoSs: the FP-EoS (van Riper 1988) and the PS-EoS (Pandharipande & Smith 1975), similar to the A-EoS and the L-EoS of Paper I (see Arnett & Bowers 1977 for the labeling of the EoSs). The FP is a soft equation of state (radius  $R = 1.06 \times 10^6 \text{ cm}$  for a  $1.4 M_\odot$  static neutron star and central density  $\rho_c = 1.27 \times 10^{15} \text{ g cm}^{-3}$ ), while the PS is stiffer ( $R = 1.64 \times 10^6 \text{ cm}$  and  $\rho_c = 3.6 \times 10^{14} \text{ g cm}^{-3}$  for the same canonical mass). In the most favorable circumstances and accreting  $0.5 M_\odot$  (an acceptable amount for the baryonic mass transferred in a LMB), a NS can spin up to a period of  $P_{\text{sh}} = 0.73 \text{ ms}$  (for FP-EoS) and of  $P_{\text{sh}} = 1.40 \text{ ms}$  (for PS-EoS). These values have been computed according to Burderi et al. (1999), who developed a semianalytical model for studying the evolution of the rotational period of a magnetic neutron star as a function of the accreted baryonic mass. The model permits the inclusion of general relativistic effects and comprises (1) the stellar deformation

(circumferential radius) as a function of angular velocity, (2) the variation of the moment of inertia in response to the mass load and to the increasing rotation, (3) the location of the marginally stable orbit for the computation of the angular momentum transfer rate in low-field NSs, and (4) the decrease of the mass-shedding period for the compact object, due to the increase of the baryonic mass by accretion.

In our statistical model of Paper I, we evolved NSs in low-mass binaries (LMBs) through the five phases of the recycling scenario. Here, we start with a population of NSs at the onset of the Roche lobe overflow (RLO) phase. The adopted parameters are shown in Table 1. Urpin et al. (1998a) calculated the tracks in the  $\mu$ - $P$  plane for a sample of pulsars, assuming different hypotheses for the binary evolution times, for the magnetic field decay and for the angular momentum transfer between the intervening plasma and the magnetosphere. Starting with pulsar parameters ( $\mu_{\text{ini}}$  and  $P_{\text{ini}}$ ) in accordance with the most updated observational analyses (Bhattacharya et al. 1992; Lorimer 1994; Hartman et al. 1997), they showed that, at the end of the wind phase, the typical NS magnetic field is about 1.5–3 orders of magnitude lower than at the onset of the pulsar phase (almost depending on the duration of wind accretion; see § 3), while the period  $P$  spreads between  $\sim 0.1$  and  $\sim 1000$  s. During the RLO accretion, the spin-up line is reached after a time  $\tau_{\text{sp}} \simeq 10^5$ – $10^6$  yr, which is shorter than the duration of the RLO accretion phase. Thus, the rotational evolution of a NS is almost independent of  $P$  at the onset of the RLO phase. Therefore, we adopted a simple flat distribution in period (see Table 1) as input parameter for the calculations, verifying that the statistical outcome of the subsequent phases are insensitive to the exact range of  $P$  and/or to its detailed initial distribution.

The logarithm of the accretion rate  $\dot{m}$  (in Eddington mass  $\dot{M}_{\text{E}}$ ) during the RLO stationary phase is randomly selected from a Gaussian distribution, with peak value ( $0.1 \dot{M}_{\text{E}}$ ) and spread  $\sigma$  (half-dex) compatible with the observed values. In fact, the typical X-ray luminosities of the stationary LMXBs cluster in the interval  $10^{36} \rightarrow 10^{38}$  ergs s $^{-1}$  (van Paradijs 1995), implying accretion rate in the range  $\sim 10^{-10} \rightarrow \sim 10^{-8} M_{\odot}$  yr $^{-1}$  (for masses  $\sim 1.4 M_{\odot}$ ). Uncertainties in distance of the sources and/or in the radiative efficiency of the accretion process could affect these estimates. We note that the typical mean accretion rates selected span the interval of values calculated by Ergma et al. (1998) within scenarios with conservative mass transfer. Low-luminosity LMXBs may exist, yet undetected, so we

explore lower mean rates on the synthesized population of recycled NSs.

As shown in Burderi et al. (1999), the minimum mass for spinning a *magnetized*  $\sim 1.40 M_{\odot}$  NS up to  $P < 10$  ms is  $\sim 0.01 M_{\odot}$  (this value doubles for unmagnetized neutron stars). We adopt that value as lower limit to the total mass accreted, in our synthesized populations. As regard to the upper limit, the maximum value of the mass transferred (1) must grant for the radial stability of the accreting NS and (2) has to be compatible with the maximum duration of the RLO phase  $\tau_{\text{RLO}}^{\text{max}}$ . For both EoSs, the first criterion is safely satisfied by assuming an upper limit of  $0.5 M_{\odot}$  (as extrapolated from Cook et al. 1994). The second request introduces a free parameter.

We considered a flat probability distribution for the logarithm of time of duration of the terminal phase of recycling, when the NS could emit as a radiopulsar. The minimum adopted value largely accounts for the time necessary to clean up the NS surroundings before the magnetic dipole emission could set in again. The maximum time is limited by the age of the disk of the galaxy, for which we put an upper limit on the total duration of the entire recycling process. The value of  $\tau_{\text{RLO}}^{\text{max}}$  could be shortened if evaporation of the companion sets in (Muslimov & Sarna 1993), and we explore accordingly values as short as  $\sim 10^7$  yr.

The behavior of the function  $g$  and the value at which it zeroes (dubbed as critical fastness parameter  $\Omega_{\text{s,crit}}$ ) are still uncertain. Therefore we adopted two different forms for  $g$ , following the suggestions of Ghosh & Lamb (1991) and of Wang (1996 and references therein). However, both calculations considered only the positive branch of the  $g$ -function, which governs the transfer of angular momentum from the disk to the NS. For a slowly rotating NS, their estimates for the torque efficiency are, respectively,  $g(\Omega = 0) = 1.17$  for Wang and  $g(\Omega = 0) = 1.40$  for Ghosh & Lamb. The predicted values of  $\Omega_{\text{s,crit}}$  cover a larger range owing to the different approximations used in the calculation. However, we noticed that our results do not change sensitively if  $\Omega_{\text{s,crit}}$  varies in the interval 0.85–1.00 (in units of the Keplerian angular velocity at the inner rim of the accretion disk) compatible with the most updated estimates (but see Li & Wang 1999 for a different view).

The shapes of the  $g$ -function near  $\Omega_{\text{s,crit}}$  have to be assumed cautiously. No fully consistent calculation of the torque function is available yet for the description of the propeller phase. In order to include this effect (especially at the end of the RLO phase), we extrapolated the known  $g$  functions to their negative branch, introducing a central

TABLE 1  
POPULATION SYNTHESIS PARAMETERS

Physical Quantity	Distribution	Values	Units
NS period at $t_0^{\text{RLOa}}$ .....	Flat	1 → 100	s
NS $\mu$ at $t_0^{\text{RLOa}}$ .....	Gaussian	$\log \langle \mu_0 \rangle = 28.5$ ; $\sigma = 0.32$	G cm $^3$
$\dot{m}$ in RLO phase <sup>b</sup> .....	Gaussian	$\log \langle \dot{m} \rangle = -1.00$ ; $\sigma = 0.50$	$\dot{M}_{\text{E}}$
Minimum accreted mass .....	One-value	0.01	$M_{\odot}$
RLO accretion phase time <sup>c</sup> .....	Flat in log	$10^6 \rightarrow \tau_{\text{RLO}}^{\text{max d}}$	yr
MSP phase time .....	Flat in log	$10^8 \rightarrow 3 \times 10^9$	yr

<sup>a</sup>  $t_0^{\text{RLO}}$  = initial time of the Roche lobe overflow phase.

<sup>b</sup> Baryonic accretion rate during the Roche lobe overflow phase.

<sup>c</sup> A maximum accreted mass of  $0.5 M_{\odot}$  is permitted during the Roche lobe overflow phase.

<sup>d</sup> Maximum duration of the Roche lobe overflow phase; typical explored values:  $5 \times 10^7$  yr,  $10^8$  yr,  $5 \times 10^8$  yr.

symmetry with respect to their zero point. This preserves continuity and derivability with the minimum number of further physical hypotheses. Different semiquantitative approximations (e.g., Menou, Esin, & Narayan 1998 adopted a linear relation between  $g$  and  $\Omega$ ) do not affect our statistical findings once  $\Omega_{s,\text{crit}}$  is close to 1.00.

### 2.3. Persistent and Nonstationary Accretion

During the RLO stage, very extended phases of constant accretion rate are quite improbable. For example, Muslimov & Sarna (1993) and Ergma et al. (1998) showed how  $\dot{m}$  can vary in LMBs under different hypotheses for the evolution of the system (conservative or nonconservative mass transfer, orbital angular momentum losses, initial orbital period, and/or secondary evolutionary stage). With the aim of exploring the effect of a decreasing  $\dot{m}$  on the population of rapidly spinning objects, we compared two possibilities: persistent accretion for a time  $\tau_{\text{RLO}}$  or persistent accretion for a shorter time followed by a transient phase mimicking the quenching of the mass transfer. We modeled the switching off of the accretion as a power-law decay for  $\dot{m}$ , investigating the effect of varying the two parameters: (1) the ratio  $\mathcal{F}_{\text{que}}$  between the duration of the quenching phase with respect to the total RLO phase and (2) the index  $\Gamma_{\text{que}}$  of the power law. Adopted values for  $\mathcal{F}_{\text{que}}$  are in the range 0.0  $\rightarrow$  0.5 and for  $\Gamma_{\text{que}}$ , from 1 (linear decay) to 10 (representative of an almost sudden switch-off). Probably the quenching of the accretion is not a smooth process but develops through alternate phases of higher and lower mass transfer rate, transforming the NS in a transient source of X-rays. Owing to the short timescales of outburst and recurrence (with respect to the duration of the whole quenching process), our crude model could also describe satisfactorily this more realistic situation. To the contrary, our model cannot account for those cases in which the accretion rate initially decreases and later increases substantially (in tight systems as indicated in Ergma et al. 1998; for MSPs recycled in intermediate-mass binaries as recently suggested in Podsiadlowski & Rappaport 1999).

We account for the angular momentum losses by propeller, both for persistent and for nonstationary accretion during phase IV. An extended spin-down phase is quite unlikely in the former case because a steady accretion rate and a reduced magnetic moment imply a very small magnetosphere. On the contrary, if, at the end of the RLO phase,  $\dot{m}$  decreases, the magnetospheric arm can increase, allowing for an efficient transfer of angular momentum from the NS outside.

## 3. MAGNETIC FIELD EVOLUTION IN LMBs

### 3.1. Physical Model

A basic assumption for the present investigation is the crustal origin of the neutron star magnetic field, i.e., it is created at the beginning of the NS's existence in its crustal layers. The onset of a thermomagnetic instability, which transforms heat into magnetic energy during the early phases, is an effective tool to produce strong fields in the crust of a NS (Urpin et al. 1986; Wiebicke & Geppert 1996). Although that instability is not yet completely understood, it is a plausible mechanism that does not depend on special assumptions and may account for the observed variety in the NS magnetic field strengths. Moreover, the assumption of a crustal magnetic field is in accordance with the gener-

ally accepted evolutionary scenarios for isolated NSs (Urpin & Kononov 1997), NSs in low-mass binaries (Urpin, Kononov, & Geppert 1998b), NSs in high-mass binaries (Urpin et al. 1998a), and millisecond pulsars (Geppert & Kononov 1998).

Since, at the beginning of the RLO phase, the anisotropies of the conductivity  $\sigma$  can be safely neglected, the evolution of the MF is governed by the induction equation

$$\frac{\partial \mathbf{B}}{\partial t} = -\frac{c^2}{4\pi} \nabla \times \left( \frac{1}{\sigma} \nabla \times \mathbf{B} \right) + \nabla \times (\mathbf{v} \times \mathbf{B}), \quad (4)$$

where  $\mathbf{v}$  is the flux velocity of the accreted matter through the crust. When considering only the evolution of an axisymmetric dipolar poloidal field, the induction equation can be simplified by introducing the vector potential  $\mathbf{A} = (0, 0, A_\varphi)$  and choosing  $A_\varphi = s(r, t) \sin \theta/r$ . With the spherical radius  $r$  and the polar angle  $\theta$ , both the radial and meridional field components can be expressed in terms of the quantity  $s(r, t)$ ,

$$B_r = \frac{2s}{r} \cos \theta, \quad B_\theta = -\frac{\sin \theta}{r} \frac{\partial s}{\partial r}, \quad (5)$$

which gives the maximum field strength at the NS surface ( $r = R$ ) by its polar value for  $B_r$ , that is  $B_s(t) = 2s(R, t)/R$ . Although in the outer layers of the crust the inflow of matter channeled by the magnetic field is certainly not radial, the mass flow will become nearly spherically symmetric in the higher density regions, where the currents are concentrated. In the approximation of a purely radial mass flow,  $\mathbf{v} = -v_r \mathbf{e}_r$ , the induction equation can be transformed to

$$\frac{\partial s}{\partial t} = \frac{c^2}{4\pi\sigma} \left( \frac{\partial^2 s}{\partial r^2} - \frac{2s}{r^2} \right) - v_r \frac{\partial s}{\partial r}, \quad (6)$$

where the flow velocity is given by the equation of continuity as

$$v_r = \frac{\dot{M}}{4\pi r^2 \rho}, \quad (7)$$

and  $\dot{M} = \dot{m} \dot{M}_E$ . While at the surface the standard boundary condition for a dipolar field applies, i.e.,  $R \partial s / \partial r + s = 0$ , the inner boundary condition is more complicated and is still a subject of scientific debates. In order to consider the possible different evolution of the NS magnetic field at the crust-core boundary, we will apply two qualitatively different inner boundary conditions. During the accretion process onto a NS, its field both diffuses and is advected toward inner layers. It is generally accepted that the core of a NS older than  $10^9$  yr is in a superfluid/superconductive (SF/SC) state, a state that will not be changed even by the intense heating during the RLO phase. Thus, in case of  $\mathbf{v} = 0$ , at the crust-core boundary, the correct boundary condition is  $s = 0$ , since the Meissner-Ochsenfeld effect prevents the magnetic field from diffusion into the core. However, in case of  $\mathbf{v} \neq 0$ , the field, frozen in on timescales of matter flow, can cross the crust-core boundary and become assimilated in the core, together with the former crustal material. Our first boundary condition (BC I) assumes that, during the process of assimilation,  $\mathbf{B}$  will be expelled immediately by the crustal material undergoing the SF/SC phase transition. Thus we define

$$\text{BC I: } s = 0 \quad \text{at } r = r_{\text{crust-core}}. \quad (8)$$

Alternatively we consider a second boundary condition (BC II), which allows an advection of the magnetic field into the core. There, it will be not further decayed owing to SC but further advected as long as accretion lasts. This assumption results in

$$\text{BC II: } s = 0 \quad \text{at } r = 0, \quad (9)$$

which may cause the occurrence of a residual field remaining constant with time (*freezing* of the field), whereas BC I allows for an exponential magnetic field decay down to zero. The situation assuming BC II has been described by Konar & Bhattacharya (1997), and we apply also their trick to simulate an effectively infinite conductivity in the assimilated core region.

For the density profile we assume that it will not be changed by the accretion of matter onto the NS. That is certainly a good approximation as long as no more than  $\sim 0.1 M_{\odot}$  has been accreted. The chemical composition and density stratification can instead vary with increasing mass load ( $0.1 \rightarrow 0.5 M_{\odot}$ ), but these changes are considered unimportant, given the other approximations introduced.

At the beginning of the RLO, the currents maintaining the magnetic field are already located close to the crust-core boundary ( $\rho_{\text{crust-core}} = 2 \times 10^{14} \text{ g cm}^{-3}$ ). Since even in the case of Eddington accretion the crust will not be heated up above  $5 \times 10^8 \text{ K}$ , the crustal matter at densities larger than  $10^{10} \text{ g cm}^{-3}$  is crystallized. Therefore, the relevant contributions to the electric conductivity in the crust are due to electron-phonon and electron-impurity scattering. Electron-phonon interactions dominate the transport at high temperatures and relatively low densities, whereas the impurity concentration determines the conductivity at lower temperatures and larger densities. The accretion-induced heating of the crust diminishes the electron-phonon conductivity considerably since it is  $\propto T^{-1}$  above the Debye temperature and  $\propto T^{-2}$  for lower  $T$ . Fujimoto et al. (1984), Miralda-Escudé, Haensel, & Paczyński (1990), and Zdunik et al. (1992) calculated the crustal temperature as a function of the accretion rate. For both the stiff and the soft NS model, we used the following fitting formula, which gives the dependence of the crustal temperature  $T$  on the accretion rate in agreement with the numerical results of the above authors (see Urpin & Geppert 1996):

$$\log T = 7.887 + 0.528(1 - e^{-0.899(q+11)}), \quad (10)$$

where  $q = \log(\dot{M}/M_{\odot} \text{ yr}^{-1})$ . For  $\log(\dot{M}/M_{\odot} \text{ yr}^{-1}) > -9.5$ , equation (10) yields probably a somewhat too small crustal temperature. We use the numerical data for the phonon conductivity  $\sigma_{\text{ph}}$  obtained by Itoh, Hayashi, & Kohyama (1993) and a simple analytical expression for the impurity conductivity  $\sigma_{\text{imp}}$  derived by Yakovlev & Urpin (1980). The total conductivity is given by

$$\frac{1}{\sigma_{\text{tot}}} = \frac{1}{\sigma_{\text{ph}}} + \frac{1}{\sigma_{\text{imp}}}. \quad (11)$$

The lowest accretion rate we will consider for the RLO phase is  $\log(\dot{M}/M_{\odot} \text{ yr}^{-1}) = -11$ , which corresponds to a crustal temperature of about  $8 \times 10^7 \text{ K}$ . For temperatures such as this and higher,  $\sigma_{\text{ph}}$  is the dominating contribution to the conductivity in the whole crust. Besides the temperature, density, and impurity concentration, the conductivity depends on the chemical composition of the crust as well. During an extended RLO phase, the whole mass of the

crust can be replaced by accreted matter. Therefore, instead of assuming that the crust is composed of cold catalyzed matter, we apply the chemical composition established by the pycnonuclear reactions in the course of the accretion (see Haensel & Zdunik 1990). The electric conductivities for the weakest and the strongest RLO accretion rates considered in this paper are shown in Figure 1.

The density profile for the soft EoS NS is given by van Riper (1988) (see Fig. 1 in Geppert & Urpin 1994), whereas the density profile for the stiff EoS NS is taken from Pandharipande & Smith (1975). The EoS valid in the core determines the thickness of the crust and hence the scale of the crustal field. Hence, apart from the accretion driven decay mechanisms, it governs strongly the field evolution: the softer the EoS, the faster the crustal field decays. This correlation is partly counterbalanced by relativistic effects that become stronger the softer the EoS is (Sengupta 1998).

In Figure 2 we show (for  $5 \times 10^6 \leq \tau_{\text{RLO}} \leq 5 \times 10^8 \text{ yr}$ ) the decay of the surface magnetic field under the influence of different accretion rates during the RLO phase both for soft and stiff EoS and for the two boundary conditions considered here. The BC I allows for an exponential decay down to zero if the accretion period is extended enough. It is clearly seen that the larger the accretion rate, the hotter the crust (see eq. [10]) and, hence, the more rapid the crustal field decays. The more rapid decay in case of the soft EoS in comparison with the stiff one is a result of the smaller spatial scale of the magnetic field. For both EoSs we see that the assumption of BC II results in a much stronger surface field. Only for nearly Eddington accretion rates and soft EoS (*lower right-hand panel*: curve labeled by  $-8.5$ ) is the very rapid field decay practically unaffected by the choice of the boundary condition. In that case, perhaps, effects of submergence play an important role because for such large

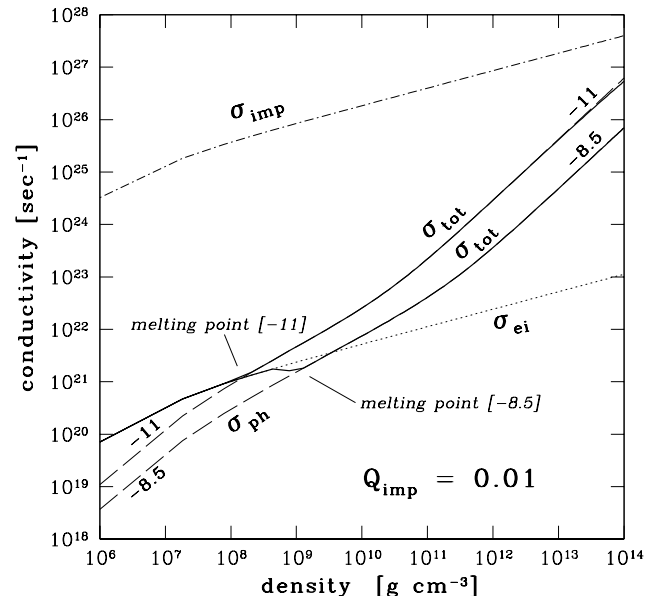


FIG. 1.—Electric conductivity in the crust as a function of the density for  $\log(\dot{M}/M_{\odot} \text{ yr}^{-1}) = -8.5$  and  $-11$ . The heavy solid lines correspond to the total conductivity  $\sigma_{\text{tot}}$ . Since the impurity conductivity ( $\sigma_{\text{imp}}$ , dot-dashed line) is not dependent on the temperature, it is the same for both accretion rates. The conductivity in the liquid region ( $\sigma_{\text{ei}}$ , dotted line) is determined by electron-ion collisions and also practically is not dependent on  $T$ , contrary to the phonon conductivity ( $\sigma_{\text{ph}}$ , dashed lines), which dominates  $\sigma_{\text{tot}}$  at highest densities. The shift of the melting point toward higher densities for higher accretion rates is seen.

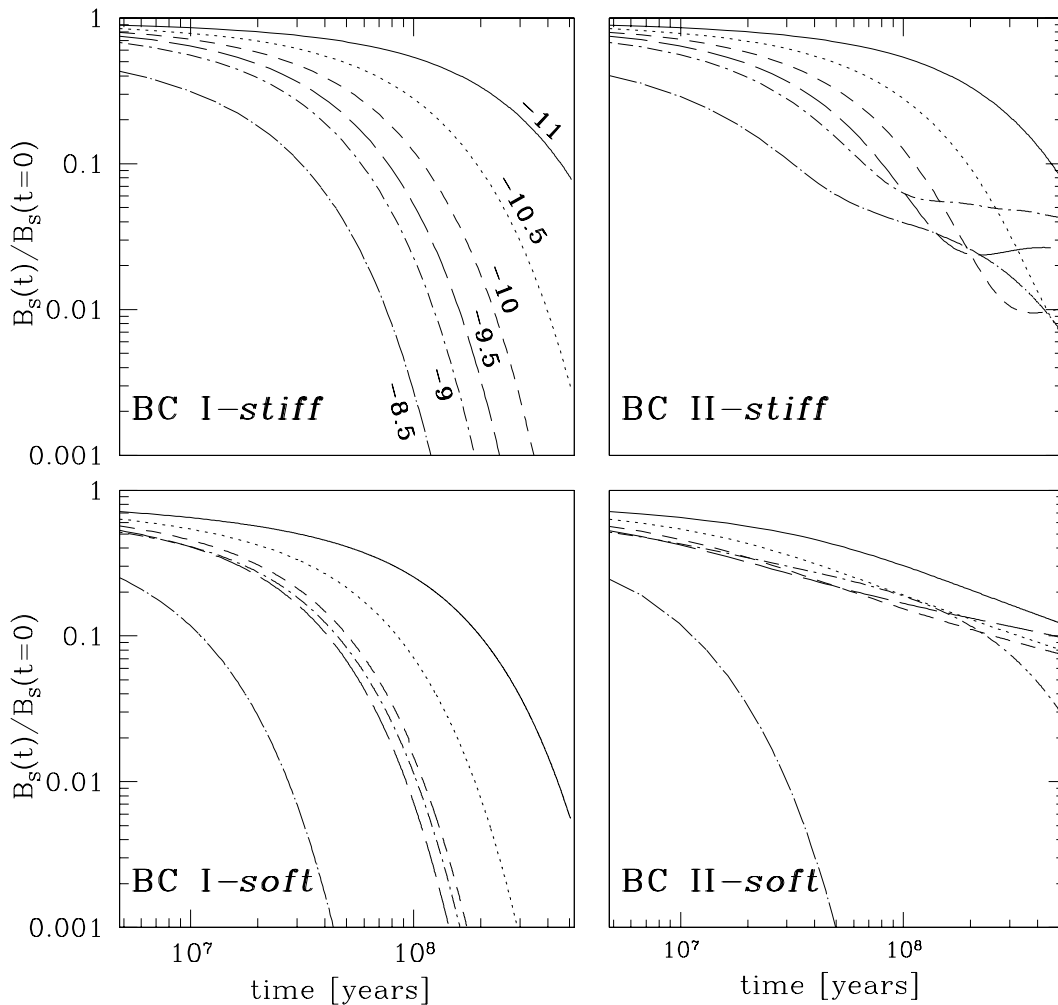


FIG. 2.—Dependence of the surface magnetic field,  $B_s(t)$ , on the time, normalized on the surface magnetic field strength at the beginning of the RLO phase ( $t = 0$ ). The different accretion rates are labelled according to  $\log(\dot{M}/M_\odot \text{ yr}^{-1})$ . The four explored cases are located here as in all the following figures: stiff EoS on the upper panels, soft EoS on the lower ones; boundary condition BC I on the left-hand panels and BC II on the right-hand panels.

accretion rates the characteristic time for the mass flow in the lower density layers of the crust is smaller than the ohmic (re-)diffusion time in that region. For the soft EoS a trend in establishing a residual field is at most suggested for  $\log(\dot{M}/M_\odot \text{ yr}^{-1}) = -10$  and  $-9.5$ . The existence of residual fields seems to be much more evident for stiff EoS. For the lowest accretion rates the velocity of mass flow at the crust-core boundary is certainly too small to create residual fields during  $\tau_{\text{RLO}} \leq 5 \times 10^8 \text{ yr}$ , and for the near-Eddington accretion, the effect of submergence acts. However, for  $\log(\dot{M}/M_\odot \text{ yr}^{-1}) = -9$ ,  $-9.5$ , and  $-10$ , the development of a residual *frozen* field is clearly seen, and its strength is positively correlated to the accretion rate, as Konar & Bhattacharya (1998) recently pointed out.

### 3.2. Values Adopted for the Synthesized Populations

The typical value of the magnetic moment  $\mu$  for the observed pulsar population lies in the range of  $10^{29.5} - 10^{31.5} \text{ G cm}^3$  (Bhattacharya et al. 1992; Lorimer 1994; Hartman et al. 1997). During the subsequent evolutionary stages in a LMB,  $\mu$  decays either by ohmic diffusion during the cooling of the NS (ejector and/or propeller phase) or by accretion-driven decay mechanisms during the comparatively extended wind accretion phase, which can last up to  $10^{10} \text{ yr}$ .

In these phases the depth of the crust initially penetrated by the magnetic field determines its strength. When the standard NS enters the RLO phase, it has an age  $\gtrsim 10^9 \text{ yr}$ , and the field has had enough time to diffuse down to the crust-core boundary, where the steep increase of the electric conductivity prevents further inward diffusion, wherever the field was initially contained. Thus, at the onset of RLO, the field is located at the core-crust boundary, and its absolute strength is the parameter to be varied in the population synthesis. Examining the various paths in the  $\mu$ - $P$  plane calculated either by Geppert & Kononov (1998) or by Urpin et al. (1998a), it appears that, at the end of the wind phase, the bulk of the evolved NSs group on the  $\mu$ -axis at values around  $10^{28} - 10^{29.5} \text{ G cm}^3$ . Such a clustering of the NSs, in a relatively narrow interval in  $\mu$ , allows us to bar the uncertainties in the magnetic evolution of the objects during the first three stages of the recycling scenario. The values  $\mu_0$  for the magnetic moment at the onset of the RLO era ( $t_0^{\text{RLO}}$ ) are selected from a Gaussian distribution (see Table 1) with a mean chosen in that interval.

## 4. RESULTS AND DISCUSSION

To execute the evolution we built a Monte Carlo code, typically using 3000 particles. The statistical analysis is per-

formed only on those NSs reaching the so-called millisecond strip at the end of the fifth stage (*radio*) of the recycling scenario, those having period  $P \leq 10.0$  ms and any value of the magnetic moment  $\mu$ . In accordance with the values of  $P_{\min}$  and  $\mu_{\min}$  (the weakest magnetic moment observed in PSR J2317+1439;  $\mu_{\min} = 7.3 \times 10^{25}$  G cm<sup>3</sup>), we divided our particles into four groups. Those filling the first quadrant in the millisecond strip ( $P \geq P_{\min}$  and  $\mu \geq \mu_{\min}$ ) behave as the known MSPs. Also, the objects belonging to the second quadrant ( $P < P_{\min}$  and  $\mu \geq \mu_{\min}$ ) should shine as pulsars (see Burderi & D’Amico 1997 and the discussion in § 1). The effective observability of the objects in the third quadrant ( $P < P_{\min}$  and  $\mu < \mu_{\min}$ ) as radio sources represents instead a challenge for the modern pulsar surveys. Most of them will be above the Chen & Ruderman (1993) death line and might have a bolometric luminosity comparable to that of the known MSPs. Thereafter we shortly refer as *sub*-MSPs to all the objects having  $P < P_{\min}$  and  $\mu$  above the death line. Objects in the fourth quadrant ( $P \geq P_{\min}$  and  $\mu < \mu_{\min}$ ) are probably radio-quiet neutron stars (RQNSs) because they tend to be closer to the theoretical death line and they are in a period range that was already searched with good sensitivity by the radio surveys.

#### 4.1. Are Submillisecond Pulsars a Natural Outcome of Evolution in LMBs?

In this section, we discuss the results of our population synthesis calculations with no inclusion of the propeller effect. We will refer to these hereafter as *standard* models. In Figure 3, we report the observed sample of MSPs and the calculated populations for the two EoSs and the two adopted boundary conditions at the crust-core interface. The input parameters are those of Table 1 with  $\tau_{\text{RLO}}^{\text{max}} = 5 \times 10^8$  yr. It appears that objects with periods  $P < P_{\min}$  are present in a statistically significant number. In effect, though the detailed distributions of particles in the millisecond strip are influenced either by the EoS and by the magnetic field decay (see also Figs. 4 and 5), *a tail of potential sub-MSPs always emerges*.

In the synthetic sample for the *soft* EoS, the “barrier” at  $P_{\text{sh}} \simeq 0.7$  ms is clearly visible in Figure 3, indicating that the field decay in long-lived persistent LMBs proceeds fast enough to allow a significant fraction of objects to attain  $P_{\text{sh}}$ . The results are more clearly illustrated in Figure 4 (*solid line*): the *soft* EoS gives rise to *period distributions that increase rather steeply toward values smaller than 2 ms*, irrespective of the adopted BCs. Instead, the boundary condi-

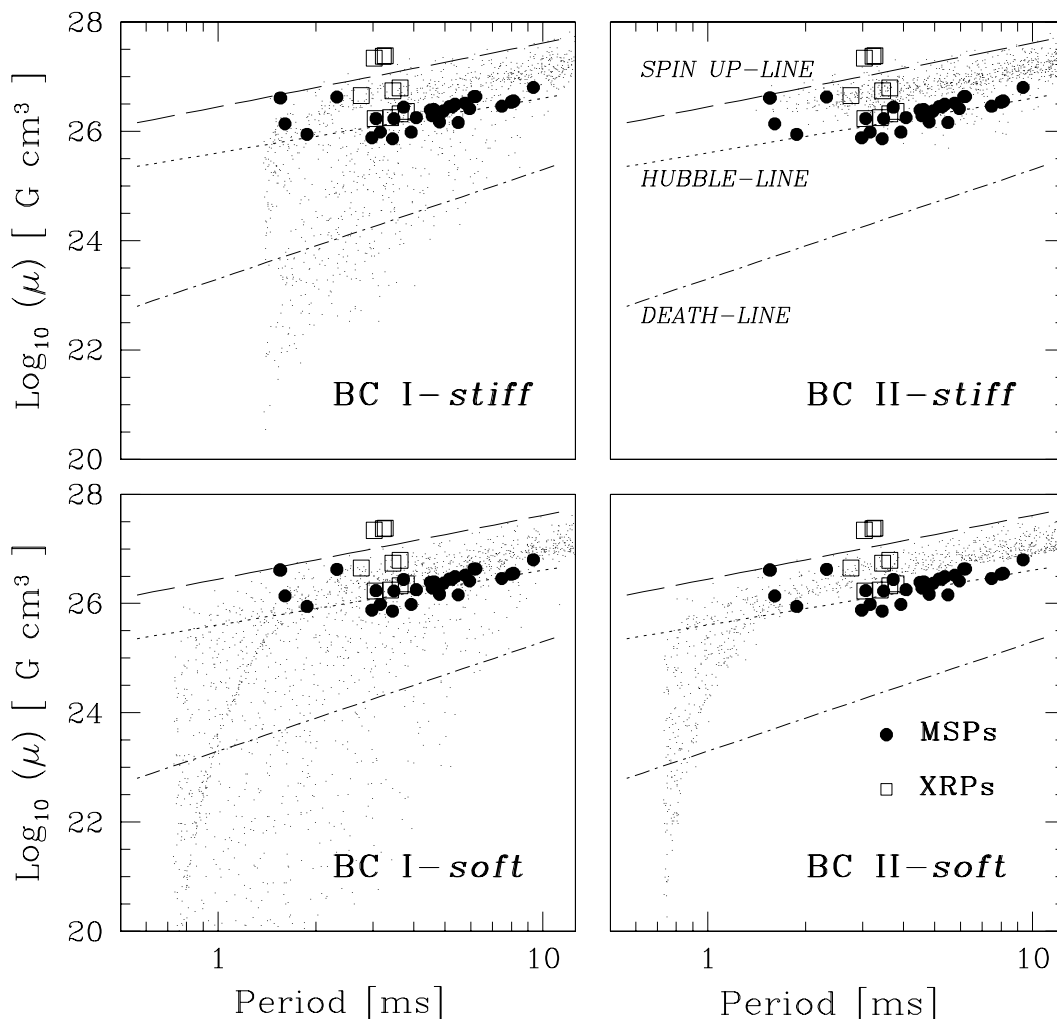


FIG. 3.—Statistical properties of the synthesized populations in the  $\mu$ - $P$  plane, for  $\langle \dot{m} \rangle = 0.1$  and  $\tau_{\text{RLO}}^{\text{max}} = 5 \times 10^8$  yr. Filled dots represent the sample of detected MSPs (on-line catalog), while open squares represent the NSs in LMBs for which the period and the magnetic field have been inferred either from the kHz QPOs seen in their X-ray power spectrum or from coherent pulsations during burst, as reported in White & Zhang (1997).

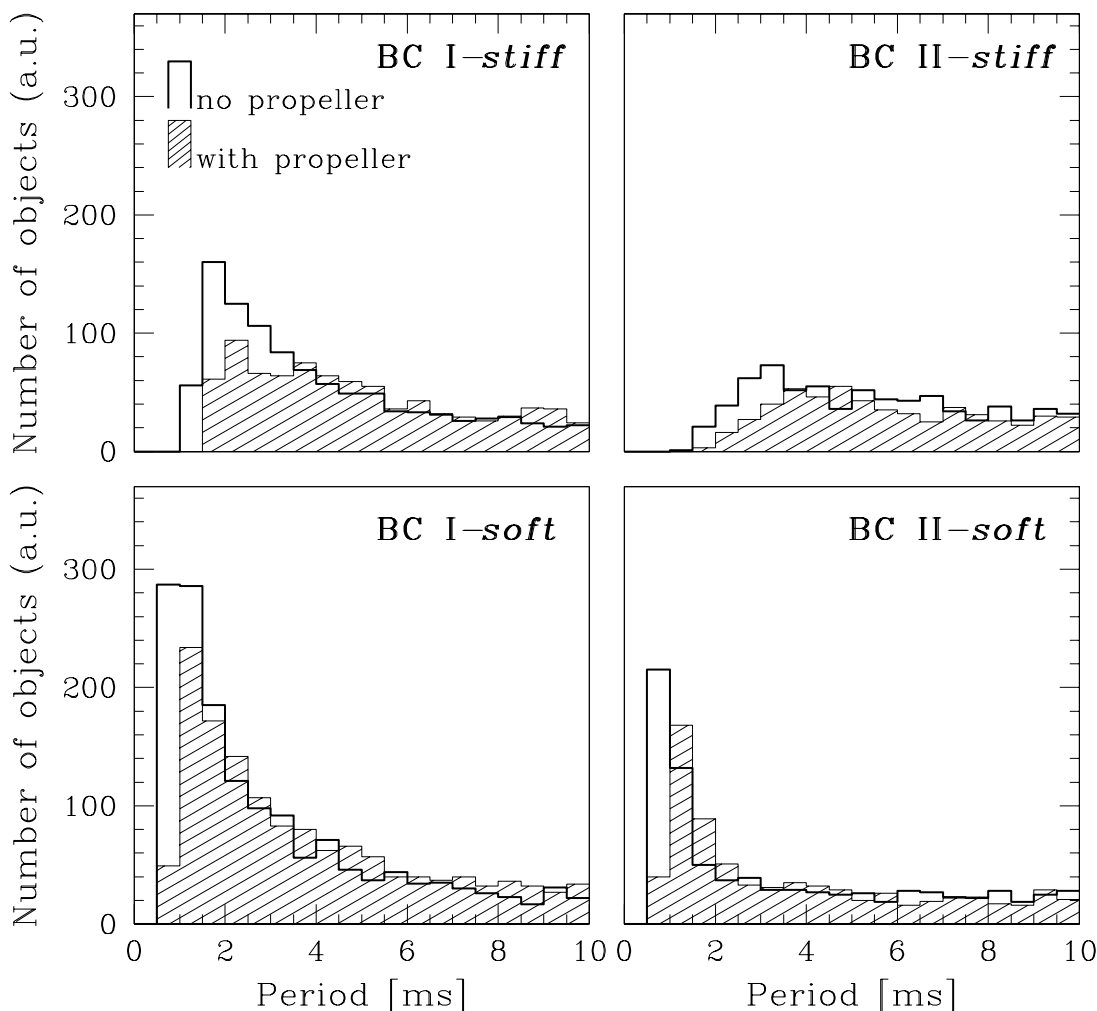


FIG. 4.—Calculated distribution of millisecond NSs as a function of the spin period  $P$ . The selected interval is  $P_{\text{sh}} < P < 10$  ms, and  $\mu$  is allowed to vary over the whole range. Solid line denotes the distribution in absence of propeller, while the dashed area gives the one with a strong propeller effect included ( $\mathcal{F}_{\text{que}} = 0.50$  and  $\Gamma_{\text{que}} = 8$ ). The absolute number of objects is in arbitrary units.

tion affects the distribution on  $\mu$ : BC II produces a smaller number of objects with low field, as the field initially decays, but, when the currents are advected toward the crust-core boundary, their decay is halted and the field reaches a bottom value. In particular, as already found in Paper I where a BC of type II was considered, the fourth quadrant in Figure 5 is underpopulated (see also Table 2).

The very *stiff* EoS permits periods  $P$  longer than 1.4 ms, but the minimum observed period  $P_{\text{min}}$  is already close to the “barrier” of mass shedding. Moreover, the field decay is established on timescales longer than for a soft EoS, and, on average, the sample of objects has a higher mean field. As a consequence, only fewer objects appear on the left of  $P_{\text{min}}$  (Fig. 3). NSs with  $\mu < \mu_{\text{min}}$  are rare objects for a BC of type II, and the ratios of *sub*-MSPs to MSPs are reduced with respect to the soft EoS (for the boundary condition BC II, we have 0.003 for the stiff EoS and 0.573 for the soft one; see Table 2 for a complete review of the results).

Major differences appear when examining Figure 4 (*solid line*): the period distribution for the stiff EoS is much flatter than that for the soft EoS, displaying a broad maximum at  $P \sim 3$  ms. It was recently claimed that X-ray sources in LMBs (possible progenitors of the MSPs; see § 4.4 for details) show rotational periods clustering in the interval

2 → 4 ms (White & Zhang 1997; van der Kluijs 1998). This effect could be explained by introducing a fine-tuned relation between  $\mu$  and  $\dot{m}$  ( $\mu \propto \dot{m}^{1/2}$ ; White & Zhang 1997). Alternatively, gravitational wave emission has been invoked, due either to the growing of  $r$ -mode instability in the accreting NS (Andersson, Kokkotas, & Stergioulas 1998) or to a thermally induced quadrupole moment in the NS crust (Bildsten 1998). Here we note that such a clustering can be a natural statistical outcome of the recycling process.

#### 4.2. Is Unsteady or Transient Accretion in LMBs a Threat to the Existence of Sub-MSPs?

The suggestion that NSs in low-mass binaries may become transiently accreting sources after having experienced a phase of persistent accretion prompted us to consider the effect of decreasing the mean accretion rate  $\dot{m}$  to mimic either the quenching of the accretion phase or the phases of quiescence in transient sources. If the magnetic field is high enough for the magnetosphere to affect the flow, the propelled matter may transfer the angular momentum of the NS outward. Therefore, we have considered the possibility that the NSs spend a fraction of the RLO phase in transit to final quiescence. The quenching of the accretion

		BC I		BC II			
<i>stiff</i>	2%	60%	1%	99%	$10^{25.8} \text{ Gcm}^3$		
	6%	32%	0%	0%			
<i>soft</i>	4%	42%	11%	57%	$10^{25.8} \text{ Gcm}^3$		
	34%	20%	32%	0%			
		1.558 ms		1.558 ms			
standard evolution							

FIG. 5.—Distributions of the synthesized NSs, derived normalizing the sample to the total number of stars with  $P < 10$  ms. We have divided the  $\mu$ - $P$  plane into four regions. As a guideline, the upper left number in each cross gives the percentage of objects having  $P < P_{\min}$  and  $\mu > \mu_{\min}$  (the typical variance is about 1%). On the left-hand side, we have indicated the EoS used. The crosses in the first column refer to the boundary condition BC I, whereas those in the second column refer to BC II.

rate was modeled with a simple power law in time with index  $\Gamma_{\text{que}}$  lasting a fraction  $\mathcal{F}_{\text{que}}$  of the duration of the RLO phase. Figures 4, 6, 7, and 8 and Table 2 show a summary of the results.

In Figure 4 the dashed areas give the distributions of the NSs at the end of evolution, including a strong propeller

phase ( $\mathcal{F}_{\text{que}} = 0.50$ ;  $\Gamma_{\text{que}} = 8$ ) during the quenching of the RLO. The emerging distributions are depleted of the fastest rotating NSs. However, it is remarkable that *for the soft EoS, the distributions preserve a maximum just about  $P_{\min}$ .*

In Figure 6 we display the distribution on  $P$  of our synthesized populations at the end of the RLO phase (including

TABLE 2  
POPULATION SYNTHESIS RESULTS

		BC I			BC II					
		Percentage Ratio			Percentage Ratio					
EoS	Number I	II/I	(II+III)/I	(III+IV)/I	Number I	II/I	(II+III)/I	(III+IV)/I	KIND OF EVOLUTION	INDEX
(1)	(2)	(3)	(4)	(5)	(6)	(7)	(8)	(9)	(10)	(11)
Stiff.....	689	4.0	14.2 (11.5)	63.5	823	0.3	0.3 (0.3)	0.0	Standard	i
	671	1.5	8.6 (6.9)	65.3	774	0.1	0.3 (0.3)	0.0	Propeller	ii
	738	0.0	8.4 (2.3)	110.3	1000	0.1	0.3 (0.3)	0.0	Low $\dot{m}$ + propeller	iii
	277	0.0	0.0	0.0	275	0.0	0.0	0.0	Short <sub>RLO</sub> + propeller	iv
	125	0.0	0.0	0.0	116	0.0	0.0	0.0	Short <sub>RLO</sub> + low $\dot{m}$ + propeller	v
Soft.....	742	10.1	91.9 (46.0)	129.0	547	19.4	74.3 (57.3)	54.9	Standard	vi
	730	8.0	83.9 (40.5)	131.1	523	16.3	73.8 (55.9)	57.5	Propeller	vii
	720	0.6	85.1 (21.1)	207.4	390	12.1	42.5 (34.2)	30.4	Low $\dot{m}$ + propeller	viii
	677	17.7	34.2 (34.2)	17.2	640	18.2	28.8 (28.8)	10.6	Short <sub>RLO</sub> + propeller	ix
	410	3.4	7.6 (7.6)	5.9	231	7.0	11.9 (11.9)	5.5	Short <sub>RLO</sub> + low $\dot{m}$ + propeller	x

NOTES.—I: Number of synthesized objects in the first quadrant ( $P > P_{\min}$  and  $\mu > \mu_{\min}$ ). These numbers are normalized to case (iii) for boundary condition BC II, set equal to 1000. II/I: Percentage ratio of the objects filling quadrant II over those filling quadrant I. (II+III)/I: Percentage ratio of the objects filling quadrants II and III over those filling quadrant I. Parentheses contain the percentage ratio of the objects having  $P < P_{\min}$  and  $\mu$  above the death line over those filling the first quadrant. (III+IV)/I: Percentage ratio of the objects filling quadrants III and IV over those filling quadrant I. Index: Index for the specific synthesized population. The different kinds of evolution are labeled as in the text.

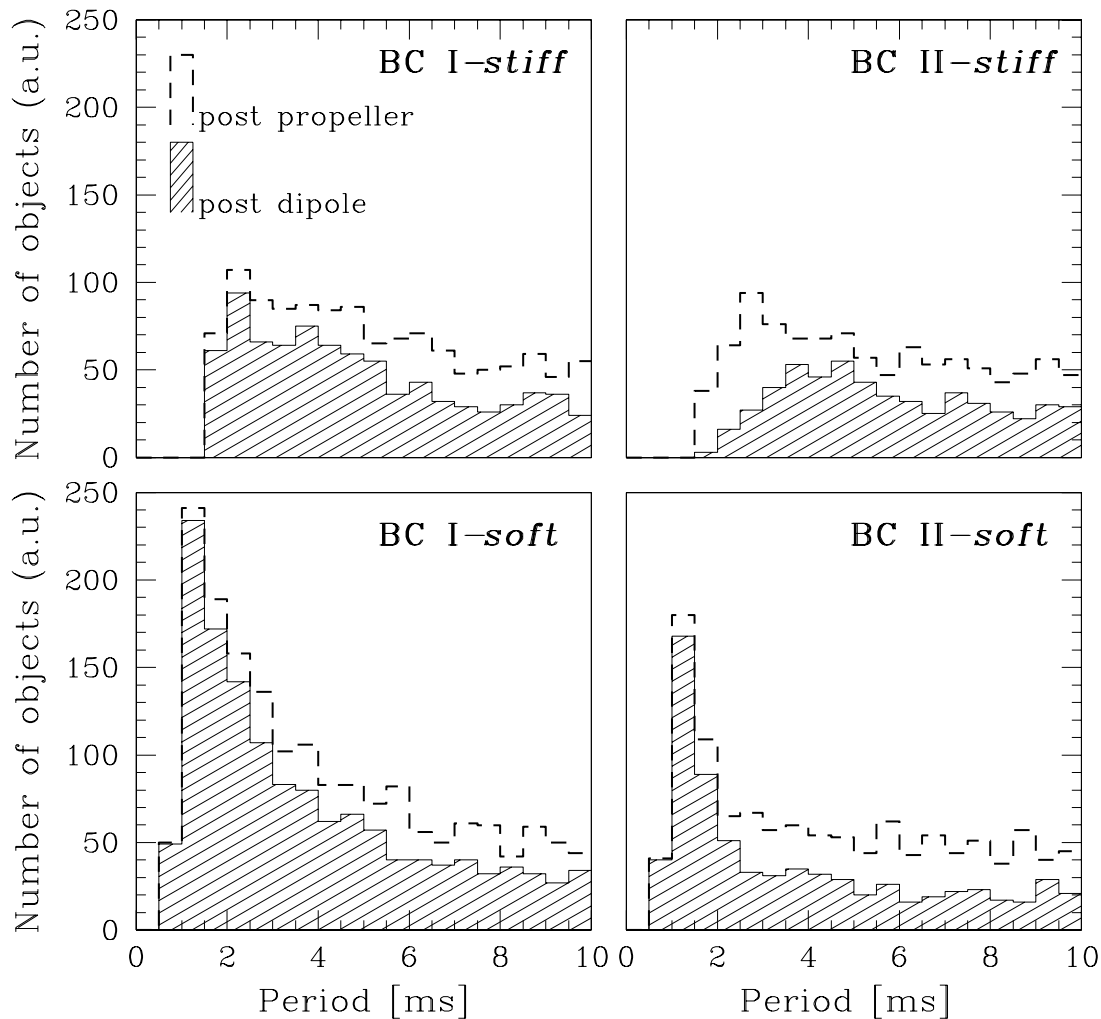


FIG. 6.—Four panels depict the distributions of NSs at the end of the propeller phase (*dashed lines*) and at the end of the magnetic dipole phase (*dashed areas*).  $\mu$  is kept constant during the radio phase. The propeller is mimicked as in the case of Fig. 4.

strong propeller: *dashed lines*) and at the end of the magnetic dipole emission phase (*dashed areas*). It appears that dipole losses produce a clear shift of the entire population toward longer periods. However, it affects preferentially the distribution of NSs at periods longer than  $\sim 4$  ms. In our simulation we have noticed that dipole losses reduce considerably the number of NSs in the millisecond strip (especially for  $\mu > \mu_{\min}$ ). In particular Figure 7 shows that dipole losses are much more effective than a mild propeller ( $\mathcal{F}_{\text{que}} = 0.25$ ;  $\Gamma_{\text{que}} = 1$ ) in drifting the overall population at  $P > 10$  ms, whereas it only slightly influences the very rapidly spinning objects.

Figure 7 also allows for the comparison of the different number of objects synthesized in the millisecond strip with different models. These numbers mainly depend on the timescale for  $\mu$  to decay down to  $\sim 10^{27.5}$  G cm<sup>3</sup>, the value requested for a particle to enter the millisecond strip: the shorter the decay timescale is, the more filled is the millisecond strip. With BC I, the soft EoS gives a number of objects that is about 50% greater than the stiff EoS. For BC II such a distinction is smoothed except for a very short RLO phase ( $\tau_{\text{RLO}}^{\text{max}} \simeq 5 \times 10^7$  yr), for which the freezing of  $\mu$  is not operating yet.

Comparing Figure 8 with Figure 5, we note that a *strong propeller can threaten the formation of NSs with  $P < P_{\min}$*

and  $\mu > \mu_{\min}$  especially in the case of the stiff EoS (see Table 2). For objects with  $\mu < \mu_{\min}$ , the spin-down torque is weaker: accordingly, quadrant III is less depleted than the second one, and a number of low magnetic field rapidly spinning NSs can survive at periods  $\simeq 1$  ms, for the soft EoS.

Our statistical analysis can provide also information on the NS mass distribution as a function of  $P$  at the end of evolution (Fig. 9). We find that the mass function steepens toward high values when  $P$  falls below  $P_{\min}$ : the distribution approaches values close to  $M \sim 1.7\text{--}1.8 M_{\odot}$  as a large mass deposition is required to spin a NS to ultrashort periods (we defer to Burderi et al. 1999 for a discussion on the minimum mass of NSs close to  $P_{\text{sh}}$ ). LMBs could harbor NSs with such high values of the mass, and a first indication comes from Casares, Charles, & Kuulkers (1998) who inferred for Cyg X-2 a lower mass limit of  $1.88 M_{\odot}$ . The action of the propeller during evolution has the clear effect of inhibiting the mass infall: the mass distribution is only slightly affected for the soft EoS, while for the stiff EoS the difference is more pronounced.

#### 4.3. A Tool for Discriminating EoS and $\mu$ -Decay ?

In this section we summarize the results of our statistical analysis considering in particular those objects having  $P <$

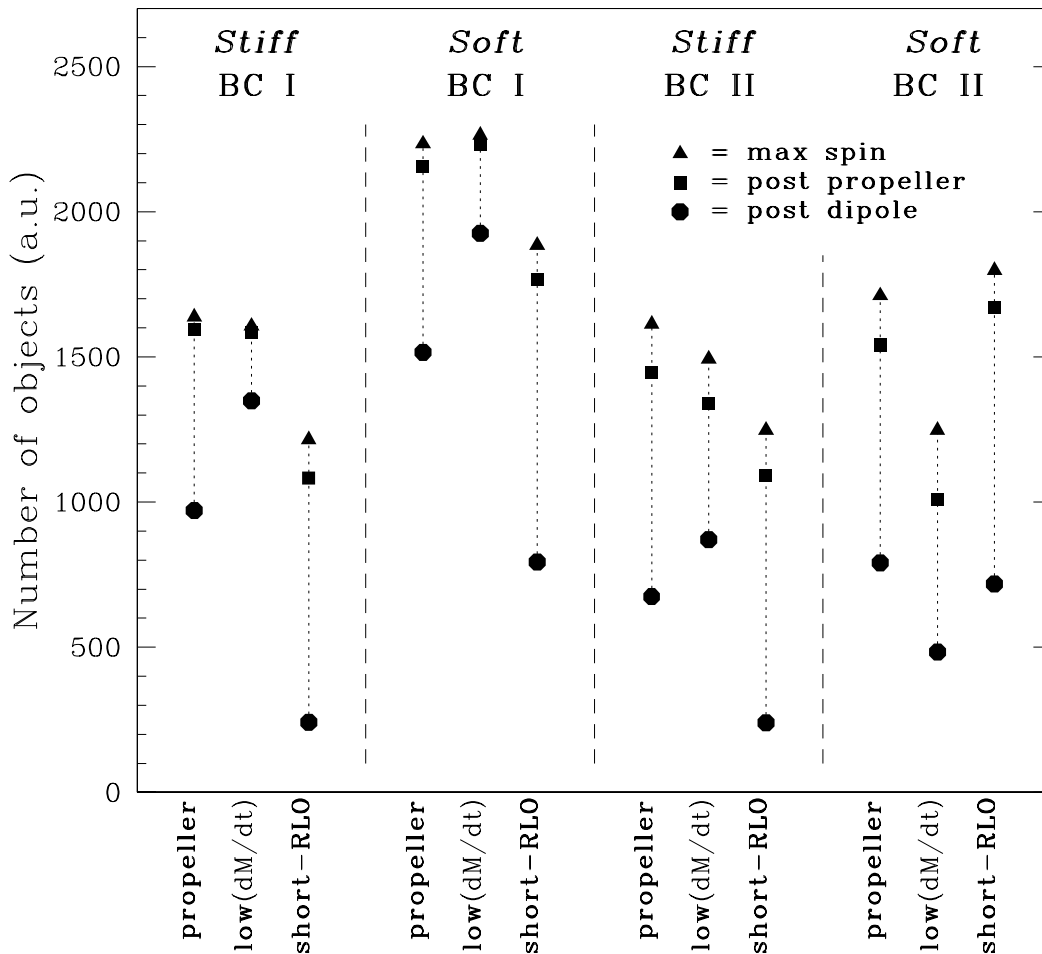


FIG. 7.—Number of synthesized objects with  $P < 10$  ms at different stages of their evolution and for different models as indicated in the labels. “Propeller” model refers to  $\tau_{\text{RLO}}^{\text{max}} = 5 \times 10^8$  yr,  $\langle \dot{m} \rangle = 0.1$  in Eddington units,  $\mathcal{F}_{\text{que}} = 0.25$ ,  $\Gamma_{\text{que}} = 1$ . For the “low( $dM/dt$ )” model we used  $\langle \dot{m} \rangle = 0.01$ , while for the “short-RLO” model we adopted  $\tau_{\text{RLO}}^{\text{max}} = 5 \times 10^7$  yr. Triangles give the number of NSs at the end of the spin-up phase during the RLO; squares give the number of NSs at the end of the propeller phase; filled dots give the number of NSs at the end of the radio phase. The numbers calculated for each model are connected by a thin dotted line. These numbers are in arbitrary units but with the same normalization for all the cases.

$P_{\text{min}}$ . Table 2 collects the main results derived for the different scenarios (indicated in col. [10]). *Standard* evolution is that discussed in § 4.1. The other cases comprise a *propeller* phase at the end of the RLO (§ 4.2): here we adopted a propeller of intermediate effectiveness ( $\mathcal{F}_{\text{que}} = 0.25$  and  $\Gamma_{\text{que}} = 1$ ). To account for the uncertainties in the distribution of the accretion rates and/or in the maximum duration of the RLO stage, we run synthesis calculations either in the case of a *low*  $\dot{m}$  ( $\dot{m} = 0.01 \dot{M}_{\text{E}}$ ) or in the case of a *short* RLO phase ( $\tau_{\text{RLO}}^{\text{max}} = 5 \times 10^7$  yr). Finally, we combined the last two hypotheses.

The results are grouped by columns according to the adopted BC and by rows as regard to the EoS. In particular, columns (2) (for BC I) and (6) (for BC II) give the number of MSPs produced during the runs, normalized to the number of MSPs (set equal to 1000) synthesized in the case labeled (iii) in column (11). These figures give an estimate of the efficiency of the recycling process in producing objects in the first quadrant. The third (for BC I) and the seventh columns (BC II) give the fraction of NSs in quadrant II relative to quadrant I. The fourth and the eighth columns (respectively, for BC I and BC II) report the fraction  $(\text{II} + \text{III})/\text{I}$ , while in parentheses we give  $f_{\text{sub}}$ , i.e., the fraction of NSs with  $P < P_{\text{min}}$  and  $\mu$  lying above the death line relative to the sample of NSs filling quadrant I.

The estimate of  $f_{\text{sub}}$  can give an indication of the fraction of *sub*-MSPs relative to the observed MSPs: if selection criteria similar to those found in the interval  $P_{\text{min}} < P < 10.0$  ms apply as well at periods below  $P_{\text{min}}$ ,  $f_{\text{sub}}$  provides an estimate of the number of pulsars that might be observable below  $P_{\text{min}}$ . We find that  $f_{\text{sub}}$  varies between 0% and  $\sim 57\%$ ; the lower figure applies only to the case of an EoS of extreme stiffness: these objects should be observable with experiments like the survey in progress at the Northern Cross Radiotelescope near Medicina (D’Amico et al. 1998), which has similar sensitivity in the MSPs and in the *sub*-MSPs range.

Inspection of the Table 2 suggests that the EoS for the nuclear matter has a major role in determining the ratio  $f_{\text{sub}}$ : the formation of a *sub*-MSP is quite a rare event, for the very stiff EoS. On the contrary, in the case of a moderately soft EoS, the *sub*-MSP population is significant, irrespective of the details of the evolutionary scenario. Thus, the detection of a significant number of *sub*-MSPs would be strongly suggestive of a not too stiff EoS. A clear distinction in the models can be seen comparing case (iv) with case (ix). If a moderate propeller takes place and the typical RLO time-scale is shorter than usually assumed, for a soft EoS,  $f_{\text{sub}} \simeq 30\%$  (irrespective the BC), while no *sub*-MSPs could appear if the nuclear matter behaves as predicted by the stiff EoS.

		BC I		BC II		
<i>stiff</i>	0%	54%	0%	100%	$10^{25.8} \text{ G cm}^3$	
	0%	46%	0%	0%		
<i>soft</i>	1%	39%	3%	61%	$10^{25.8} \text{ G cm}^3$	
	21%	39%	28%	8%		
		1.558 ms		1.558 ms		
<b>strong propeller</b>						

FIG. 8.—Distributions of the synthesized NSs, when a strong propeller ( $\mathcal{F}_{\text{que}} = 0.50$ ;  $\Gamma_{\text{que}} = 8$ ) is applied. Labels as in Fig. 5

The details of the evolution can blend the outcome of the statistical analysis preventing a clear distinction between the equations of state when based on the simple ratio  $f_{\text{sub}}$  (e.g., cases [i], [ii], and [iii] vs. case [x] for the BC I). The boundary condition for the magnetic field at the crust-core interface weakly affects the figures of Table 2 (except for case [viii]) when considering only the objects filling quadrants I and II (compare cols. [2] and [3] with cols. [6] and [7]). Owing to their effects on the decay of the surface magnetic field, *the differences between the two BCs are revealed mainly in the synthesized populations having  $\mu < \mu_{\text{min}}$ .*

#### 4.4. Very Low Magnetic Field NSs Spinning at Millisecond Periods?

Except for the most unfavorable case (very stiff EoS and BC II), all our synthesis runs produce a significant amount of objects with  $\mu < \mu_{\text{min}}$  (see quadrants III and IV in Figs. 5 and 8). Their period distribution is very sensitive to the adopted internal boundary condition for the magnetic field diffusion at the crust-core interface. BC II clearly favors rapidly rotating objects ( $P \lesssim 1.5$  ms), quadrant IV in Figures 5 and 8 being (scarcely) populated only in the case of a very strong propeller. For BC I the distributions are broader, and the stiffer the EoS is, the more depleted is quadrant III. In principle, such a distinction could allow a discrimination between the two BCs.

From the observational point of view, very low magnetized NSs in quadrant IV (upon which we focus in this section) might be elusive sources. Irrespective of the selection effects or survey sensitivity thresholds, these objects might be rather close to the theoretical death line to be observable as radio, and it is not clear if we can observe them in the X-ray band.

Recently a neutron star rotating in the millisecond interval (SAX J1808.4–3658 with  $P = 2.49$  ms) has been detected in X-rays (Wijnands & van der Kluis 1998). It is in a binary system with a low-mass companion (Chakrabarty & Morgan 1998), which transfers mass to the compact object. As the rotational period is known, one can constrain the surface magnetic field of the accreting NS (Psaltis & Chakrabarty 1999). An upper limit on  $\mu$  relies on the requirement (1) that accretion is not centrifugally inhibited at the minimum accretion rate at which coherent pulsations are detected. The standard disk-magnetosphere model (Pringle & Rees 1972) interprets coherent X-ray pulsations as being due to a complete or a partial funneling of the disk plasma along the NS magnetic field lines. Many improvements had to be added to this model (Ghosh & Lamb 1991 for a review) to account for the variety of observations (e.g., Bildsten 1997); but in this framework, (2) a rotating NS can appear as an accretion-powered pulsar only if the magnetic moment is strong enough to terminate the Keplerian disk above the stellar surface (Psaltis & Chakrabarty 1999; Burderi & King 1998). This requirement translates to a lower boundary on the possible value of  $\mu$ . For the case of SAX J1808.4–3658, Psaltis & Chakrabarty (1999) found  $3 \times 10^{25} \lesssim \mu \lesssim 10^{27} \text{ G cm}^3$ , with a preferred value about a few times  $10^{26} \text{ G cm}^3$ . So, this object seems to be placed near the separation of quadrants I and IV. Alternative models, not related or poorly related to  $\mu$ , could explain coherent X-ray modulation at the NS spin frequency (e.g., azimuthal variation in optical depth for absorption or scattering) from which no further constraints on  $\mu$  arise.

Already in the first half of the 1990s, the spin periods for a handful of NSs in low mass X-ray binaries have been inferred either from coherent pulsations during type I bursts

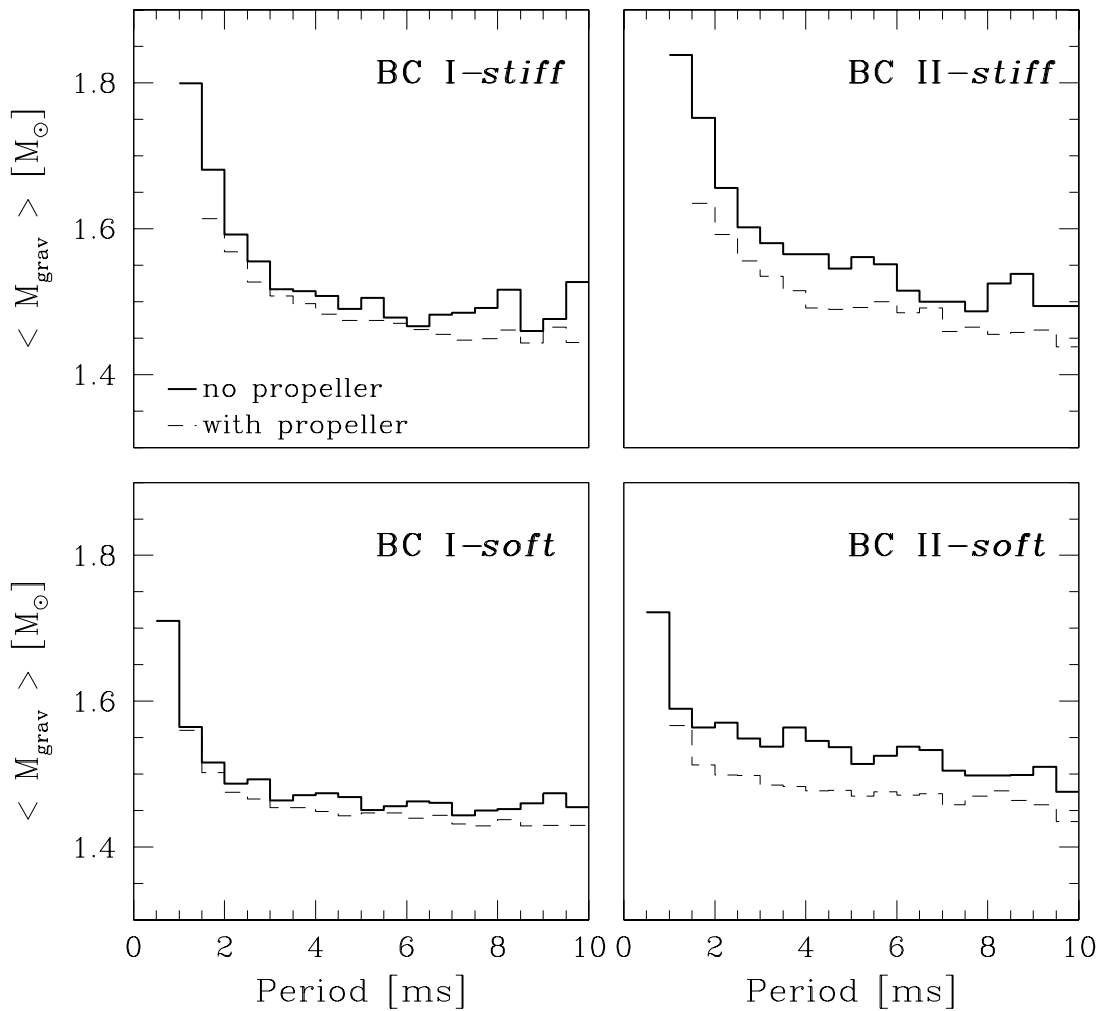


FIG. 9.—Average gravitational masses of the reaccelerated NSs as a function of their final spin period  $P$ .  $\mu$  is allowed to vary over the whole range, and the synthesized NSs are binned in 0.5 ms wide intervals. The initial mass of the static NSs is set equal to  $1.40 M_{\odot}$  for all the cases. Thick solid line denotes the mass distribution in absence of propeller, whereas thin dashed line gives the one with a strong propeller effect included ( $\mathcal{F}_{\text{que}} = 0.50$  and  $\Gamma_{\text{que}} = 8$ ).

or, indirectly, from the so-called kHz QPOs (see van der Klips 1998 for a review). In the latter case, the paradigm is the so-called beat frequency model, in which the frequency difference  $\Delta\nu_{\text{qpo}}$  between the two peaks appearing in the X-ray power spectrum of the source is representative of the spin frequency of the NS or of an overtone (Miller, Lamb, & Psaltis 1998). From the inferred spin, and assuming that these NSs rotate at about their equilibrium period (that is, near their competing spin-up line), one can estimate (through condition [1]) the value of  $\mu$ . As a representation, in Figure 3, we display (*open squares*) the positions of the NSs of this group in the  $\mu$ - $P$  plane, adopting the values of White & Zhang (1997 and reference therein for a discussion of the errors in the determination of  $P$  and  $\mu$ ). It appears that no X-ray source shows  $\mu < \mu_{\text{min}}$ .

Prompted by the evidence of a value for  $\Delta\nu_{\text{qpo}}$  that is not constant (Psaltis et al. 1998; Mendez et al. 1998), other models for explaining the kHz QPOs have been proposed. For instance, Stella & Vietri (1999) interpret the upper QPO frequency  $\nu_2$  as being due to matter inhomogeneities orbiting the NS at the inner disk boundary (just as in the standard beat frequency model), while the lower QPO frequency  $\nu_1$  is produced by the periastron precession at the inner edge of the accretion disk. Apart from negligible corrections (due to the effect of the NS rotation on the exterior

metric), the observed difference  $\Delta\nu_{\text{qpo}} = \nu_2 - \nu_1$  is unrelated to the spin frequency of the NS. Since  $P$  is not constrained by the observation, condition (2) for a lower limit on  $\mu$  does not apply any more. Hence we argue also that the magnetic moment estimates become questionable in this framework. As a consequence, some of the sources shown in Figure 3 could be misplaced in the  $\mu$ - $P$  plane and, when accretion halts, they could eventually enter the category of low magnetic field NSs. A similar suggestion was raised by Li & Wang (1999), who constructed refined slim disk models in LMBs, incorporating the effects of both magnetic field and general relativity: for the kHz QPO sources, he found values of the surface magnetic field smaller than the previous authors. If this is the case, the values of  $\mu$  in kHz QPO sources ( $\lesssim 10^{25} \text{ G cm}^3$ ) are systematically weaker than those of MSPs sample, and these X-ray-emitting objects would populate our quadrant IV.

As a general comment on the observability of low magnetic field NSs in the X-ray band, we note that if the capability of coherently emitting X-rays pulses requires high enough values of  $\mu$ , missing rotating NSs with  $P$  close to a millisecond would not be surprising: as already shown in Burderi et al. (1999) and here confirmed, only a rapid and substantial decay of  $\mu$  allows a NS to reach  $P < P_{\text{min}}$ . Therefore, low magnetic field, rapidly spinning NSs could

be just those not showing coherent X-ray pulsations. Instead, the signature of very rapidly spinning objects might hopefully emerge from low-amplitude features in their power spectrum, not related to coherent modulation of the X-ray brightness.

### 5. CONCLUSIONS

The population synthesis calculation has shown the following:

1. Detailed models for the decay of the crustal magnetic field, including also refined relativistic corrections, show the presence of a tail in the period distribution of the synthetic NSs population at periods shorter than 1.558 ms.

2. For the soft EoS, and irrespective of the boundary condition at the crust-core interface for the magnetic field evolution, recycling in LMBs gives rise to a NS distribution that is increasing toward shorter periods, and a clear barrier is present at the minimum period for mass shedding. For the stiff EoS, the distribution is flatter.

3. If NSs at the end of the persistent accretion in a LMB experience a phase of smooth decrease of the accretion rate (to mimic transient sources and/or quenching of accretion), the magnetospheric propeller produces a depletion of rapidly spinning NSs, but, at least for the soft EoS, it preserves a distribution that peaks at periods  $\sim 1.5$  ms.

4. The estimated fraction of *sub*-MSPs over the entire MSPs population varies between 0% and  $\approx 50\%$ . The adopted EoS and the parameters for the recycling play an important role in determining those percentages. The detection of such rapid rotating compact objects represents a challenge for the modern searches.

5. The models for the decay of a crustal magnetic field predict the existence of spun-up NSs with very low magnetic moment: their period distribution is a neat signature for the physics at the crust-core interface.

The first two authors want to acknowledge the hospitality of the members of the Astrophysikalisches Institut Potsdam during the early phase of this work.

### REFERENCES

- Alpar, M. A., Cheng, A. F., Ruderman, M. A., & Shaham, J. 1982, *Nature*, 300, 728
- Andersson, N., Kokkotas, K. D., & Stergioulas, N. 1998, preprint (astro-ph/9806089)
- Arnett, W. D., & Bowers, R. L. 1977, *ApJS*, 33, 415
- Bhattacharya, D. 1995, in *X-ray Binaries*, ed. W. H. G. Lewin, J. van Paradijs, & E. P. J. van den Heuvel (Cambridge: Cambridge Univ. Press), 5
- Bhattacharya, D., & Srinivasan, G. 1995, in *X-Ray Binaries*, ed. W. H. G. Lewin, J. van Paradijs, E. P. J. van den Heuvel (Cambridge: Cambridge Univ. Press), 495
- Bhattacharya, D., & van den Heuvel, E. P. J. 1991, *Phys. Rep.*, 203, 1
- Bhattacharya, D., Wijers, R., Hartman, J., & Verbunt, F. 1992, *A&A*, 254, 198
- Bildsten, L. 1997, *ApJS*, 113, 367
- . 1998, *ApJ*, 501, L89
- Bisnovatyi-Kogan, G. S., & Komberg, B. V. 1975, *Soviet Astron.*, 18, 217
- Blandford, R. D., Applegate, J. H., Hernquist, L. 1983, *MNRAS*, 204, 1025
- Burderi, L., & D'Amico, N. 1997, *ApJ*, 490, 343
- Burderi, L., Di Salvo, T., Robba, N. R., Del Sordo, S., Santangelo, A., & Segreto, A. 1998, *ApJ*, 498, 831
- Burderi, L., & King, A. R. 1998, *ApJ*, 505, L135
- Burderi, L., Possenti, A., Colpi, M., Di Salvo, T., & D'Amico, N. 1999, *ApJ*, 519, 285
- Casares, J., Charles, P., & Kuulkers, E. 1998, *ApJ*, 493, L39
- Chakrabarty, D., & Morgan, E. H. 1998, *Nature*, 394, 345
- Chen, K., & Ruderman, M. 1993, *ApJ*, 402, 264
- Cook, G. B., Shapiro, S. L., & Teukolsky, S. A. 1994, *ApJ*, 423, L117
- Cordes, J. M., & Chernoff, D. F. 1997, *ApJ*, 482, 971
- D'Amico, N., et al. 1998, in *Neutron Stars and Pulsars*, ed. N. Shibasaki, N. Kawai, S. Shibata, & T. Kifune (Tokyo: Universal Academy), 235
- Ding, K. J., Chen, K. S., & Chau, H. F. 1993, *ApJ*, 408, 167
- Ergma, E., & Sarna, M. J. 1996, *MNRAS*, 280, 1000
- Ergma, E., Sarna, M. J., & Antipova, J. 1998, *MNRAS*, 300, 352
- Frank, J., King, A. R., & Raine, D. 1992, *Accretion Power in Astrophysics* (Cambridge: Cambridge Univ. Press)
- Fujimoto, M., Hanava, T., Iben, I., Jr., & Richardson, M. 1984, *ApJ*, 278, 813
- Geppert, U., & Konenkov, D. 1998, in *Neutron Stars and Pulsars*, ed. N. Shibasaki, N. Kawai, S. Shibata, & T. Kifune (Tokyo: Universal Academy), 31
- Geppert, U., & Urpin, V. 1994, *MNRAS*, 271, 490
- Ghosh, P., & Lamb, F. K. 1991, in *Neutron Stars: Theory and Observation*, ed. J. Ventura & D. Pines (Dordrecht: Kluwer), 363
- Haensel, P., & Zdunik, J. L. 1990, *A&A*, 227, 431
- Hartman, J. W., Verbunt, F., Bhattacharya, D., & Wijers, R. A. M. J. 1997, *A&A*, 322, 477
- Illarionov, A., & Sunyaev R. 1975, *A&A*, 39, 185
- Itoh, N., Hayashi, H., & Kohyama, Y. 1993, *ApJ*, 418, 405
- Kalogera, W., & Webbink, R. F. 1996, *ApJ*, 458, 301
- . 1998, *ApJ*, 493, 351
- King, A. R., Frank, J., Kolb, U., & Ritter, H. 1997a, *ApJ*, 484, 844
- King, A. R., Kolb, U., & Szuszkiewicz, E. 1997b, *ApJ*, 488, 89
- Konar, S., & Bhattacharya, D. 1997, *MNRAS*, 284, 311
- . 1998, preprint (astro-ph/9808119)
- . 1999, preprint (astro-ph/9812035)
- Li, X. D., & Wang, Z. R. 1999, preprint (astro-ph/9901083)
- Lipunov, V. M. 1992, *Astrophysics of Neutron Stars* (Berlin: Springer)
- Lorimer, D. R. 1994, Ph.D. Thesis, Univ. of Manchester
- Mendez, M., van der Klis, R., Wijnands, R., Ford, R. C., van Paradijs, J., & Vaughan, B. A. 1998, preprint (astro-ph/9807281)
- Menou, K., Esin, A. A., & Narayan, R. 1998, preprint (astro-ph/9810323)
- Miller, M. C., Lamb, F. K., & Psaltis, D. 1998, *ApJ*, 508, 791
- Miralda-Escudé, J., Haensel, P., & Paczyński, B. 1990, *ApJ*, 362, 572
- Miri, M. J., & Bhattacharya, D. 1994, *MNRAS*, 269, 455
- Muslimov, A. G., & Sarna, M. J. 1993, *MNRAS*, 262, 164
- Pandharipande, V., & Smith, R. 1975, *Nucl. Phys. A*, 237, 507
- Phinney, E. S., & Kulkarni, S. R. 1994, *ARA&A*, 591
- Podsiadlowski, Ph., & Rappaport, S. 1999, preprint (astro-ph/9906045)
- Possenti, A., Colpi, M., D'Amico, N., & Burderi, L. 1998, *ApJ*, 497, L97 (Paper I)
- Pringle, J. E., & Rees, M. J. 1972, *A&A*, 21, 1
- Psaltis, D., et al. 1998, *ApJ*, 501, L95
- Psaltis, D., & Chakrabarty, D. 1999, *ApJ*, 521, 332
- Ruderman, M. A., & Sutherland, P. G. 1975, *ApJ*, 196, 51
- Ruderman, M. A., Zhu, T., & Chen, K. 1998, *ApJ*, 492, 267
- Sang, Y., & Chanmugam, G. 1987, *ApJ*, 323, L61
- Sengupta, S. 1998, *ApJ*, 501, 792
- Srinivasan, G., et al. 1990, *Curr. Sci.*, 59, 31
- Stella, L., & Vietri, M. 1999, *Phys. Rev. Lett.*, 82, 17
- Stergioulas, N., & Friedman, J. 1995, *ApJ*, 444, 306
- Sturrock, P. A. 1971, *ApJ*, 164, 529
- Urpin, V. A., & Geppert, U. 1996, *MNRAS*, 278, 471
- Urpin, V. A., & Konenkov, D. 1998a, *MNRAS*, 295, 907
- Urpin, V. A., & Konenkov, D. 1997, *MNRAS*, 284, 741
- Urpin, V. A., Konenkov, D., & Geppert, U. 1998b, *MNRAS*, 299, 73
- Urpin, V. A., Levshakov, S. A., & Yakovlev, D. G. 1986, *MNRAS*, 219, 703
- van der Klis, M. 1998, in *The Many Faces of Neutron Stars*, ed. M. A. Alpar, R. Buccheri, & J. van Paradijs (Dordrecht: Kluwer), 337
- van Paradijs, J. 1995, in *X-Ray Binaries*, ed. W. H. G. Lewin, J. van Paradijs, & E. P. J. van den Heuvel (Cambridge: Cambridge Univ. Press), 536
- . 1996, *A&A*, 464, L139
- van Riper, K. A. 1988, *ApJ*, 329, 339
- Wang, Y.-M. 1996, *ApJ*, 465, L111
- Webbink, R. F., Rappaport, S. A., & Savonije, G. J. 1983, *ApJ*, 270, 678
- White, N. E., & Zhang, W. 1997, *ApJ*, 490, L87
- Wiebicke, H. J., & Geppert, U. 1996, *A&A*, 309, 203
- Wijnands, R., & van der Klis, M. 1998, *Nature*, 394, 344
- Yakovlev, D., & Urpin, V. 1980, *Soviet Astron.*, 24, 303
- Zdunik, J., Haensel, P., Paczyński, B., & Miralda-Escudé, J. 1992, *ApJ*, 384, 129